Int. J. Heat Mass Transfer. Vol. 34, No. 10, pp. 2555–2570, 1991
Printed in Great Britain

0017–9310/91 $3.00 + 0.00

An investigation of transient three-dimensional buoyancy-driven flow and heat transfer in a closed horizontal annulus

KAMBIZ VAFAI and JAVAD ETTEFAGH
Department of Mechanical Engineering, The Ohio State University, Columbus, OH 43210, U.S.A.

(*Received* 30 *May* 1990 *and in final form* 19 *November* 1990)

Abstract—Buoyancy-driven flow and heat transfer in a horizontal annulus bounded by two impermeable boundaries in the axial direction are numerically investigated in this work. A transient three-dimensional analysis of the end effects on heat transfer and the corresponding flow field is presented. The effects of the axial impermeable boundaries are shown to be characterized by retardation of the flow field through the viscous shearing force in regions near the end walls. The results show that the temperature distribution remains unchanged in the core region provided that the annulus length to outer radius ratio is larger than a critical value. Flow and temperature fields are found to be symmetrical with respect to the mid-axial plane of the annulus. A number of interesting features resulting from the sudden heating of the inner cylinder are presented. Finally, a thorough presentation of formation of flow and temperature fields as a result of the sudden heating of the inner cylinder is given.

1. INTRODUCTION

BUOYANCY-driven flow and heat transfer in an annulus bounded by two horizontal cylinders have been the subject of a number of investigations in the past two decades. This is due to the relevance of such a geometry in a number of technologically important problems such as, nuclear reactors, thermal storage systems, cooling of electronic components, aircraft cabin insulation, underground electrical transmission lines, etc. A comprehensive literature survey concerning this configuration has been presented by Kuehn and Goldstein [1]. In most of these studies, the flow is assumed to be invariant in the axial direction which leads to a two-dimensional modeling of the problem. However, due to the viscous shearing effects at the end walls, the three-dimensional analysis is necessary and unavoidable for many practical applications where the annuli has a finite axial length. A reflection through the available literature reveals that three-dimensional investigations are quite limited due to difficulties encountered in successful implementation of the numerical schemes for such flow fields.

Although there exists a number of studies concerning three-dimensional fluid flow and heat transfer in rectangular cavities [2], only a few three-dimensional investigations on buoyancy-driven convection in a concentric cylindrical annulus exist. In one such study Ozoe *et al.* [3] utilized the vorticity-vector potential approach to solve the buoyancy-induced flow problem in vertical annular space heated from below. Numerical calculations were performed for $Ra = 6 \times 10^3$, $Pr = 10$, and radius ratio of 2. The circulation pattern was found to consist of a symmetrical set of roll cells. Ozoe *et al.* [4] investigated the effects of inclination angle for the same problem. They reported that, as the heated surface was inclined from the lower horizontal position to an upper horizontal position, the mean Nusselt number at first decreased, then increased and finally decreased to unity as the mode of circulation switched from a symmetrical array of roll cells to distorted and oblique roll cells to a single circulation. Takata *et al.* [5] performed a study of natural convection in an inclined cylindrical annulus with heated inner and cooled outer cylinders only for a very high Prandtl number fluid. In another investigation, Fusegi and Farouk [6] considered a limited analysis of the three-dimensional natural convection in a horizontal annulus with the primary emphasis placed on the steady state results.

In our investigation the transition three-dimensional governing equations are also formulated in terms of vorticity and vector potential. However, a modified form of ADI has been utilized. The original method by Douglas [7], when applied to the heat conduction equation in a rectangle, is a perturbation of the Crank–Nicolson difference equation and is second-order accurate both in space and time. Douglas [8] pointed out that the obvious generalization of the above method to three space variables is not stable for a large ratio of the time increment to the square of the space increment. The second alternating direction method can be applied to three-dimensional problems and was so presented in the work of Douglas and Rachford [9]. A modified form of this method has been adopted in the present work. The results in the present work show that convection in the axial direction is strongly influenced by boundary effects and the

NOMENCLATURE

$\mathbf{g}$	body force vector [m s^{-2}]
g	gravitational acceleration [m s^{-2}]
L	axial length of the annulus [m]
Nu	Nusselt number, equation (26)
Pr	Prandtl number, ν/α
R^*	radial coordinate [m]
r	dimensionless radial coordinate, R^*/R_2^*
Ra	Rayleigh number, $g\beta R_2^{*2}\Delta T/\alpha\nu$
t^*	time [s]
t	dimensionless time, $t^*\alpha/R_2^{*2}$
T	temperature [K]
ΔT	temperature difference, $T_1 - T_2$ [K]
$\mathbf{u}$	dimensionless velocity vector, $\mathbf{u}^*R_2^*/\alpha$
$\mathbf{u}^*$	velocity vector [m s^{-1}]
Z	axial coordinate [m]
z	dimensionless axial coordinate, Z^*/R_2^{*2}.

Greek symbols

α	thermal diffusivity [m^2 s^{-1}]
β	thermal expansion coefficient of fluid [K^{-1}]
ζ	vorticity
θ	dimensionless temperature, $(T-T_2)/(T_1-T_2)$
μ	dynamic viscosity [kg m^{-1} s^{-1}]
ν	kinematic viscosity [m^2 s^{-1}]
ρ	density [kg m^{-3}]
ϕ	angular coordinate
Ψ	vector potential.

Subscripts

1	inner cylinder
2	outer cylinder
i	nodal index in the r-direction
j	nodal index in the ϕ-direction
k	nodal index in the z-direction
r	radial component
z	axial component
ϕ	angular component.

existence of a complex double-helix three-dimensional flow pattern inside the annulus is illustrated. A thorough presentation of formation of flow and temperature fields as a result of the sudden heating of the inner cylinder is given in the present work and it is shown that the temperature distribution remains unchanged in the core region provided that the annulus is long enough.

2. ANALYSIS

The geometric model and the coordinate system (R, ϕ, Z), for the present work are shown in Fig. 1. The fluid is lodged between two concentric horizontal cylinders with an inner radius R_1, outer radius R_2, and an axial length of L. The heated inner cylinder surface and the cooled outer cylinder surface are kept at constant temperature T_1 and T_2, respectively. The two axial ends of the annulus are assumed to be impermeable and adiabatic. Due to the symmetric nature of the flow field with respect to a vertical plane crossing the center of the cylinders, the computations were performed for the $0 \leqslant \phi \leqslant \pi$ region. The transformed dimensionless governing equations in terms of vorticity and a vector potential are established as

$$\frac{\partial\theta}{\partial t} + (\mathbf{u}\cdot\nabla)\theta = \nabla^2\theta \tag{1}$$

$$\frac{\partial\zeta_r}{\partial t} + (u\cdot\nabla)\zeta_r - (\zeta\cdot\nabla)u_r = Pr\left(\nabla^2\zeta_r - \frac{\zeta_r}{r^2} - \frac{2}{r^2}\frac{\partial\zeta_\phi}{\partial\phi}\right) - Pr\,Ra\sin\phi\frac{\partial\theta}{\partial z} \tag{2}$$

$$\frac{\partial\zeta_\phi}{\partial t} + (u\cdot\nabla)\zeta_\phi - (\zeta\cdot\nabla)u_\phi + \frac{u_\phi\zeta_r - u_r\zeta_\phi}{r} = Pr\left(\nabla^2\zeta_\phi - \frac{\zeta_\phi}{r^2} + \frac{2}{r^2}\frac{\partial\zeta_r}{\partial\phi}\right) - Pr\,Ra\cos\phi\frac{\partial\theta}{\partial z} \tag{3}$$

$$\frac{\partial\zeta_z}{\partial t} + (u\cdot\nabla)\zeta_z - (\zeta\cdot\nabla)u_z = Pr\,\nabla^2\zeta_z + Pr\,Ra\left(\sin\phi\frac{\partial\theta}{\partial r} + \frac{1}{r}\cos\phi\frac{\partial\theta}{\partial\phi}\right) \tag{4}$$

$$\nabla^2\Psi_r + \frac{2}{r}\frac{\partial\Psi_r}{\partial r} + \frac{\Psi_r}{r^2} + \frac{2}{r}\frac{\partial\Psi_z}{\partial z} + \zeta_r = 0 \tag{5}$$

$$\nabla^2\Psi_\phi - \frac{\Psi_\phi}{r^2} + \frac{2}{r^2}\frac{\partial\Psi_r}{\partial\phi} + \zeta_\phi = 0 \tag{6}$$

$$\nabla^2\Psi_z + \zeta_z = 0 \tag{7}$$

$$u_r = \frac{1}{r}\frac{\partial\Psi_z}{\partial\phi} - \frac{\partial\Psi_\phi}{\partial z} \tag{8}$$

$$u_\phi = \frac{\partial\Psi_r}{\partial z} - \frac{\partial\Psi_z}{\partial r} \tag{9}$$

$$u_z = \frac{\Psi_\phi}{r} + \frac{\partial\Psi_\phi}{\partial r} - \frac{1}{r}\frac{\partial\Psi_r}{\partial\phi} \tag{10}$$

where the non-dimensional variables in the above equation are defined by

$$r = \frac{R^*}{R_2^*}, \quad z = \frac{Z^*}{R_2^*} \tag{11}$$

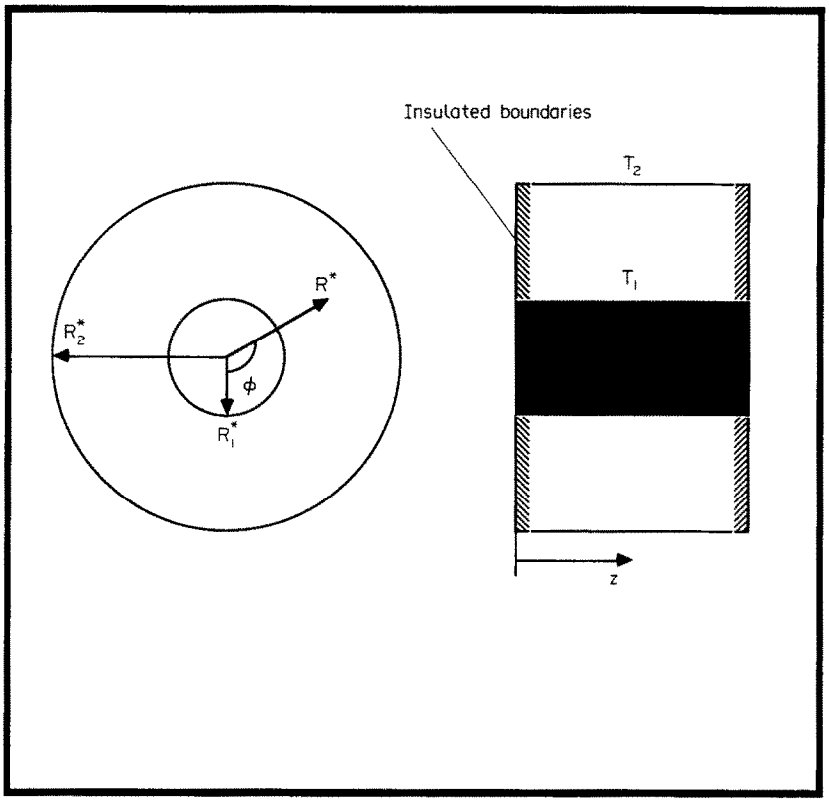

FIG. 1. Schematic of the horizontal annulus with impermeable axial boundaries.

$$u = \frac{u^* R_2^*}{\alpha}, \quad t = \frac{t^* \alpha}{R_2^{*2}} \tag{12}$$

$$\theta = \frac{T - T_2}{T_1 - T_2}. \tag{13}$$

In the above equations Ψ denotes the vector potential and ζ refers to the vorticity and the rest of the variables are defined in the Nomenclature. The above ten coupled partial differential equations for ten unknowns along with the specification of the proper boundary conditions describe the physics of the convective flow and heat transfer processes and complete the formulation of the problem.

2.1. *Boundary conditions*

On the inner and outer cylinder surfaces, the dimensionless temperatures are θ_1 and θ_2, respectively. On the axial impermeable wall the normal derivative of temperature is zero. On all rigid and impermeable surfaces, the three components of the velocity are zero. The vorticity boundary conditions are determined from the velocity gradients in the usual manner. Following the work of Hirasaki and Hellums [10] the normal gradient of the normal component of the vector potential is set to zero and the components of the vector potential tangential to the surface are also taken to be zero. Therefore, the boundary conditions at $r = R_1^*/R_2^*$ or 1 can be written as

$$u_r = u_\phi = u_z = 0 \tag{14}$$

$$\zeta_r = 0, \quad \zeta_\phi = -\frac{\partial u_z}{\partial r}, \quad \zeta_z = \frac{\partial u_\phi}{\partial r} \tag{15}$$

$$\frac{\partial}{\partial r}(r\Psi_r) = \Psi_\phi = \Psi_z = 0 \tag{16}$$

$$\theta = \theta_1 \quad \text{or} \quad \theta_2. \tag{17}$$

Since no flow crosses the top and bottom angular symmetry planes, the angular velocity vanishes on that plane. The angular derivatives of the remaining velocity components and temperature also vanish on the angular symmetry plane. The boundary conditions at $\phi = 0$ or π are then found to be

$$\frac{\partial u_r}{\partial \phi} = u_\phi = \frac{\partial u_z}{\partial \phi} = 0 \tag{18}$$

$$\zeta_r = \frac{\partial \zeta_\phi}{\partial \phi} = \zeta_z = 0 \tag{19}$$

$$\Psi_r = \frac{\partial \Psi_\phi}{\partial \phi} = \Psi_z = 0 \tag{20}$$

$$\frac{\partial \theta}{\partial \phi} = 0. \tag{21}$$

At the end walls all the velocity components are zero.

The boundary conditions at $z = 0$ or L/R_2 are then found to be

$$u_r = u_\phi = u_z = 0 \tag{22}$$

$$\zeta_r = -\frac{\partial u_\phi}{\partial z}, \quad \zeta_\phi = \frac{\partial u_r}{\partial z}, \quad \zeta_z = 0 \tag{23}$$

$$\Psi_r = \Psi_\phi = \frac{\partial \Psi_z}{\partial z} = 0 \tag{24}$$

$$\frac{\partial \theta}{\partial z} = 0. \tag{25}$$

Since there are two kinds of temperature boundary conditions (specified temperature on the cylindrical surface portion and adiabatic on the axial plane portion) imposed on the corners in the angular direction, a multi-valued procedure similar to one used in ref. [11] has been utilized here. The same approach is also employed for treating the vorticity discontinuity at these locations.

2.2. *Heat transfer calculations*

The local Nusselt number for this problem is defined as the ratio of the actual to the conduction heat transfer. That is

$$Nu = \frac{q_{\text{actual}}}{q_{\text{cond.}}} \tag{26}$$

where

$$q_{\text{cond.}} = \frac{2\pi k L(T_1 - T_2)}{\ln(R)} \quad \text{and} \quad R = \frac{R_2^*}{R_1^*}. \tag{27}$$

The mean Nusselt number is defined as the angular average of the local Nusselt numbers at the mid axial

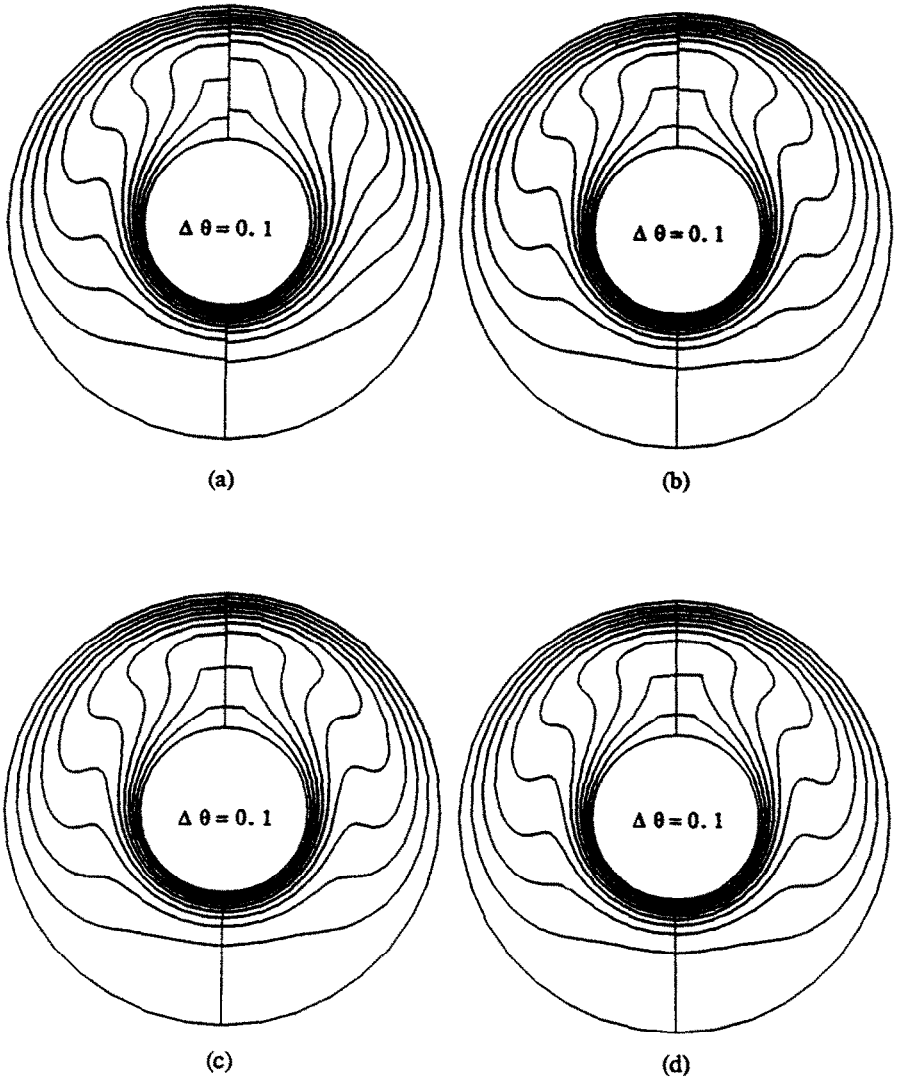

FIG. 2. Isotherms for $Ra = 4.3 \times 10^4$ at different axial positions on the right and at mid axial plane on the left: (a) $z = L/2, 0$; (b) $z = L/2, L/8$; (c) $z = L/2, L/4$; (d) $z = L/2, 3L/8$.

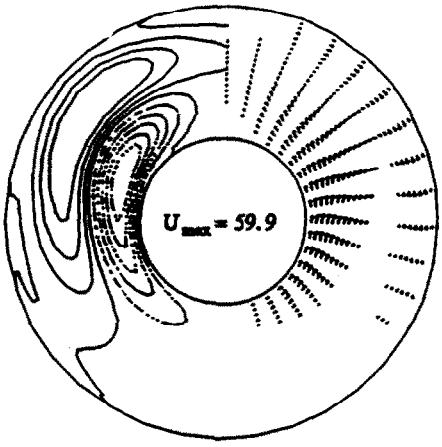

FIG. 3. Flow patterns for $Ra = 4.3 \times 10^4$ at different axial positions: (a) $z = L/40$; (b) $z = L/2$.

plane. The mean Nusselt numbers, $\overline{Nu}_1$, $\overline{Nu}_2$, in terms of dimensionless variables are defined as

$$\overline{Nu}_1 = \frac{-1}{\pi}\int_0^{\pi} R \ln(R) \left.\frac{\partial\theta}{\partial r}\right|_{r=R} \mathrm{d}\phi \qquad (28)$$

$$\overline{Nu}_2 = \frac{-1}{\pi}\int_0^{\pi} R \ln(R) \left.\frac{\partial\theta}{\partial r}\right|_{r=1} \mathrm{d}\phi. \qquad (29)$$

3. RESULTS AND DISCUSSION

The four parabolic equations (1)–(4) are solved by the modified form of the three-dimensional ADI method developed by Brian [12]. At each time step, the three elliptic equations (5)–(7) are solved by the three-dimensional extrapolated Jacobi scheme. The remaining equations (8)–(10) are solved by the central difference approximation technique.

Various combinations of mesh sizes were used to select one which produces grid independent results. Initially, the number of grids in the angular direction was set to 19 to examine the grid dependency of the results for the number of grids in the other directions. The number of grids in the radial direction was varied from 13 to 25, and 31 with 21 points in the axial direction. The calculation performed on a $25 \times 19 \times 21$ grid relative to a $13 \times 19 \times 21$ grid system yielded a 9% change in the mean Nusselt number and 6% in the maximum value of the stream function at the mid axial plane. The numerical results based on a $31 \times 19 \times 21$ grid did not show any appreciable changes, 0.4% in the mean Nusselt number and 0.1% in the maximum value of the stream function at the mid axial plane, relative to the $25 \times 19 \times 21$ grid distribution.

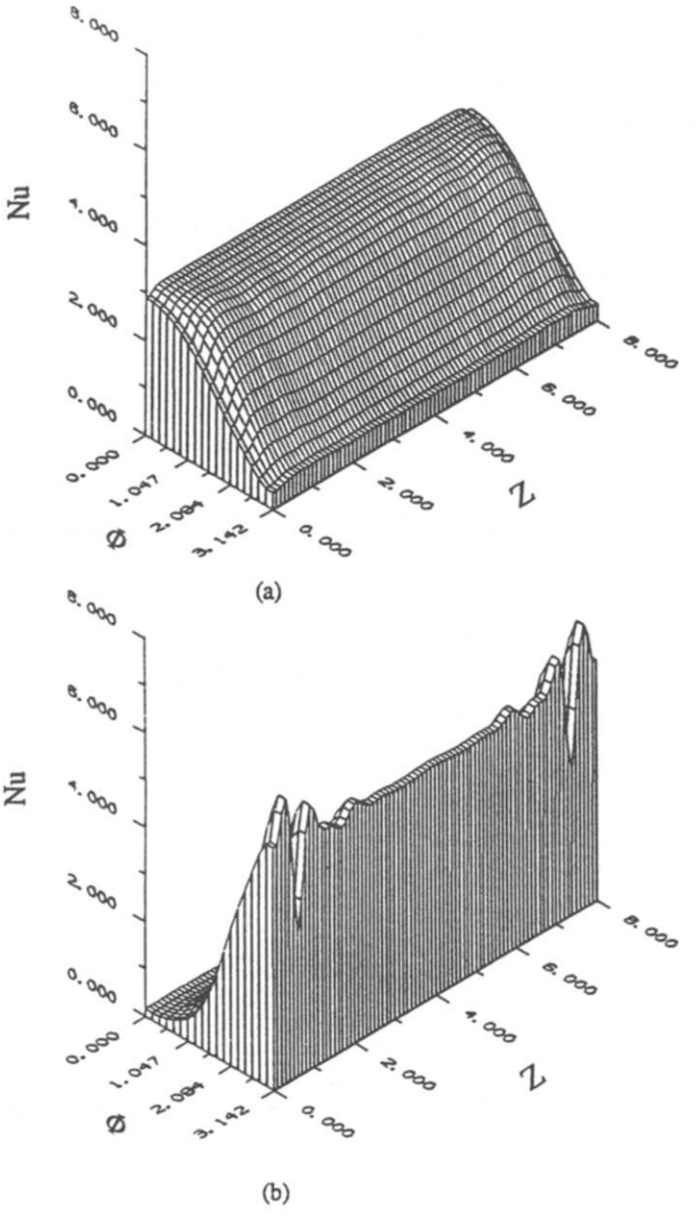

FIG. 4. The distribution of local Nusselt number for $Ra = 4.3 \times 10^4$: (a) inner cylinder; (b) outer cylinder.

To check the grid dependency in the axial direction, the number of grids was varied from 21 to 41, and 81 with 25 points in the radial direction. The calculation performed on a $25 \times 19 \times 41$ relative to a $25 \times 19 \times 21$ grid system resulted in a 4% change in the mean Nusselt number and a 2% change in the maximum value of the stream function at the mid axial plane. The number of grids in the axial direction was further increased from 41 to 81 points. For the low Rayleigh number cases there were essentially no changes while, for the high Rayleigh number flows there was only 0.5% variation in the mean Nusselt number and virtually no changes in the maximum value of the stream function at the mid axial plane relative to the results with 41 points in the axial direction.

Next, the number of grids in the angular direction was varied from 19 to 37 with 25 and 81 points in the radial and axial directions, respectively. Again for the low Rayleigh number cases there were no changes while, for the higher Rayleigh number flows an extremely small refinement in the flow field was observed. Therefore, a $25 \times 19 \times 41$ grid system was adopted for the low Rayleigh number flows. The use of a $25 \times 37 \times 81$ grid system for the high Rayleigh number case resulted in obtaining heat transfer and flow field results that are in very good agreement

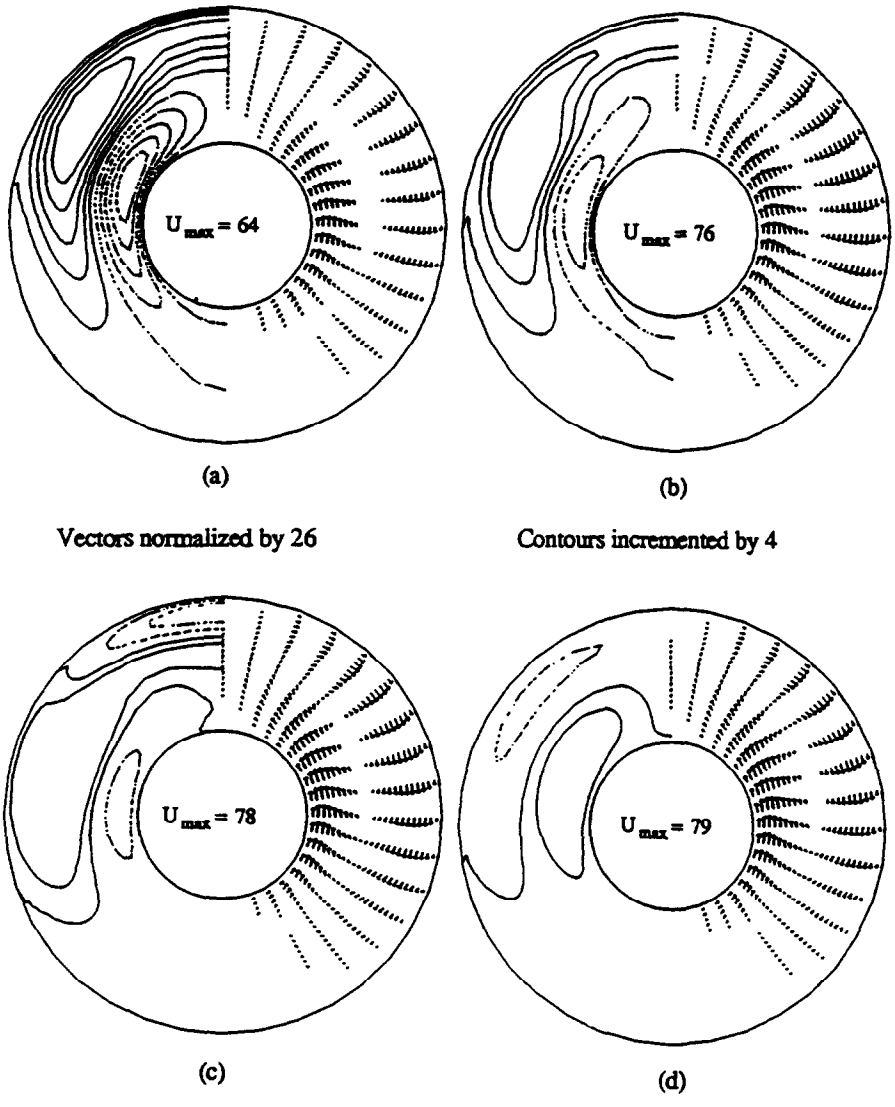

FIG. 5. Flow patterns for $Ra = 4.3 \times 10^4$ at different axial positions: (a) $z = 3L/80$; (b) $z = 3L/40$; (c) $z = L/10$; (d) $z = 17L/80$.

with the reported steady state results in the literature. Numerical tests were also performed with the above-mentioned grid distribution and different time steps sizes. It was determined that, a time increment of 2×10^{-4} had to be used in order to obtain a time step-independent solution. The numerical computations were carried out on a Cray-YMP. The typical CPU time required for the converged solutions was about 20 min.

Numerical simulations of buoyancy-driven flow in a horizontal cylindrical annulus were performed successfully over a range of Rayleigh numbers. The results were obtained for cases with inner cylinder surface temperature of $\theta_1 = 1$, and an outer cylinder surface temperature which was equal to that of the ambient temperature $\theta_2 = 0$ and using air as the working fluid. In all cases, the full transient characteristics of fluid flow and heat transfer inside the annulus were investigated. The fluid within the annulus was initially taken to be stationary and at a uniform ambient temperature. Since one of the objectives of this investigation was to compare the numerical solution with the available experimental and numerical results, the outer cylinder to inner cylinder radius ratio of 2.6 (this radius ratio was used in the two-dimensional work of Kuehn and Goldstein [1]) was considered. To accurately detect the two-dimensional nature of the flow field in the core region, an annulus with length to outer radius ratio of at least 4 was used. It should be noted that in a related study Tsui and Tremblay [13] also investigated the transient two-dimensional natural convection in a horizontal annulus.

The results of this investigation are presented at selected planes normal to the axial direction. The tem-

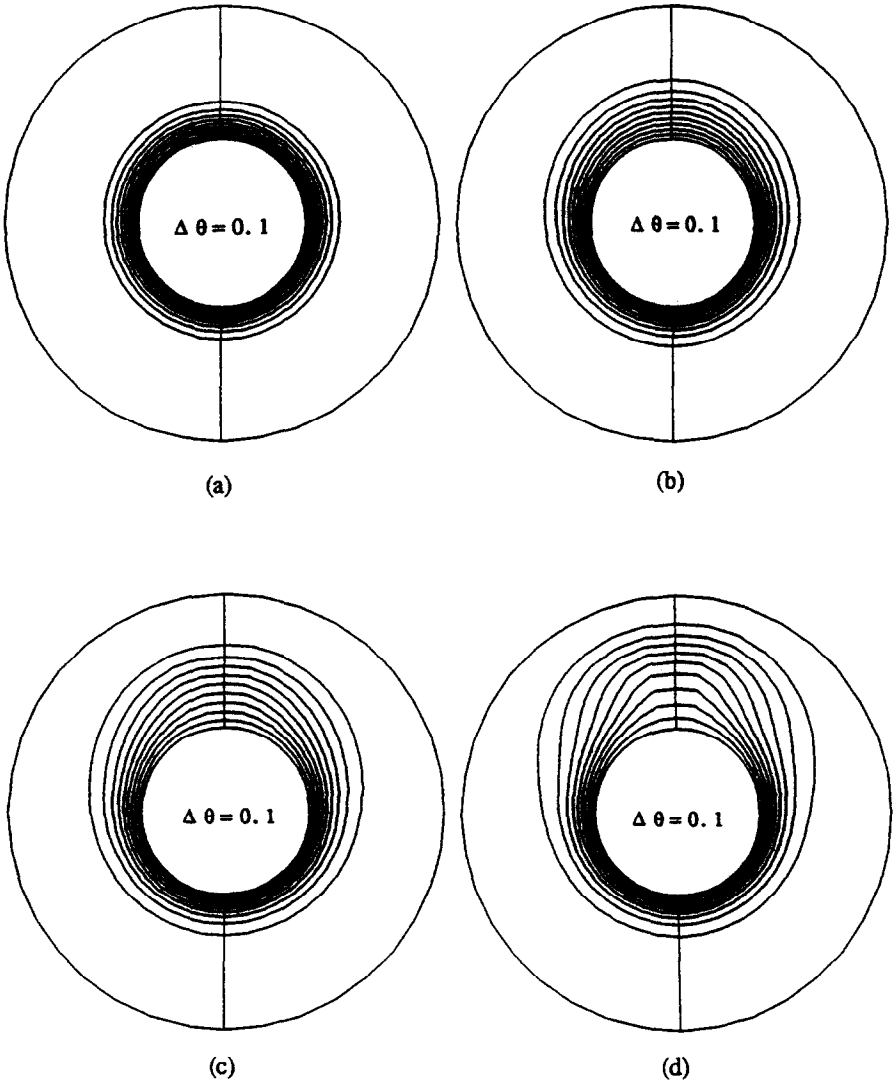

FIG. 6. Isotherms for $Ra = 4.3 \times 10^4$ at $z = 3L/8$ on the right and at mid axial plane on the left for different time steps: (a) $t = 10\Delta t$; (b) $t = 20\Delta t$; (c) $t = 30\Delta t$; (d) $t = 40\Delta t$.

perature distribution is presented in terms of isotherms at these planes. The velocity vectors composed of radial and angular components of the velocity field, as well as the contours of the axial component, are presented side by side to facilitate the flow field visualization. The dotted lines in the contours of the axial component represent the negative contours while the positive contours are drawn as solid lines. In our convention, the negative and positive axial velocity contours would illustrate areas within which the fluid is moving into (negative z-axis) or out of the plane, respectively. The local heat transfer from inner and outer cylinders is presented by three-dimensional surface plots of the corresponding Nusselt numbers. The flow pattern at the mid axial plane where the axial component of velocity vanishes, is directly presented in terms of streamlines. This is because the flow becomes two-dimensional at the core region, provided that the annulus is long enough.

The results for the case of $Ra = 5 \times 10^2$ at the mid axial plane (for brevity not presented here) indicated the stable crescent-shaped flow pattern. The isotherms were made up of concentric circles inside the annulus. This is because the velocities were too small to affect the temperature distribution and consequently the heat transfer mechanism is mainly by conduction. As the Rayleigh number is increased from 5×10^2 to 4.3×10^3, the velocity field starts to influence the temperature distribution in the annulus. However, conduction is still a major mode of heat transfer inside the annulus. As the Rayleigh number is increased the center of rotation for the crescent-shaped flow moves upward in the angular direction. In order to verify the symmetrical nature of the flow field with respect to

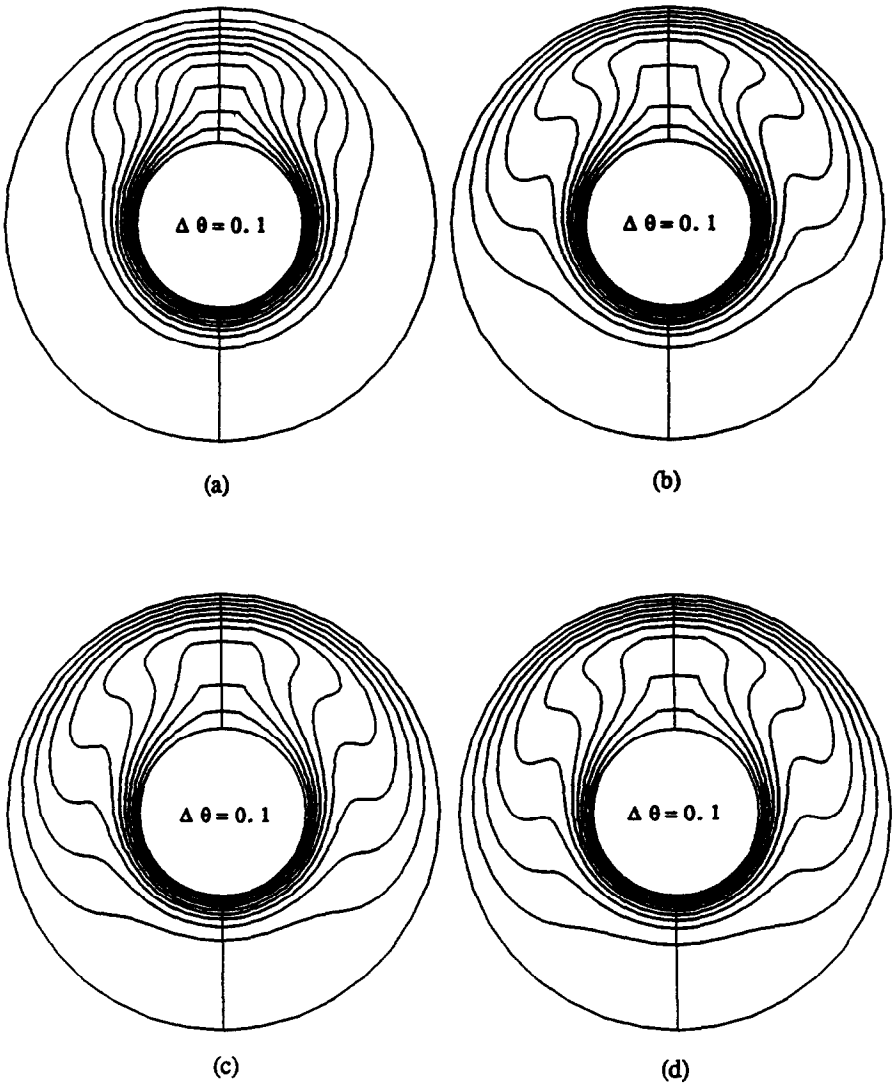

FIG. 7. Isotherms for $Ra = 4.3 \times 10^4$ at $z = 3L/8$ on the right and at mid axial plane on the left for different time steps: (a) $t = 50\Delta t$; (b) $t = 100\Delta t$; (c) $t = 150\Delta t$; (d) $t = 200\Delta t$.

the mid axial plane and the extent of the two-dimensionality of the flow field in the core region, temperature distributions for $Ra = 4.3 \times 10^3$ at several different paired positions along the axial direction were investigated. These locations were symmetrical with respect to the mid axial plane and were situated at axial positions including, and away from, the end walls of the annulus. Our investigation clearly established the symmetry of the isotherms with respect to the mid axial plane of the annulus. Furthermore, the temperature distribution within the core region of the annuli was found to be independent of the axial position. Consequently, the problem could be treated as two-dimensional convection in the R–ϕ plane within the core region. However, the isotherms at the end walls were significantly different from the isotherms at the mid axial plane. This is due to the boundary effects at the end walls which enhance the role of axial convection.

To examine the extent of this core region, i.e. the region within which the flow is essentially two-dimensional; temperature distributions at several paired positions along the axial direction were also investigated for $Ra = 4.3 \times 10^4$. These locations were chosen at axial positions including and away from the left end wall, 1/8 of the annulus length apart. Figures 2(a)–(d) illustrate the temperature distribution at these locations, respectively. In these figures, the isotherms at the mid axial plane are presented on the left-hand side while the corresponding isotherms at the cited locations are displayed on the right-hand side. The shape of the isotherms clearly shows that heat is being extracted from the lower part of the inner cylinder and convected to the upper part of the outer

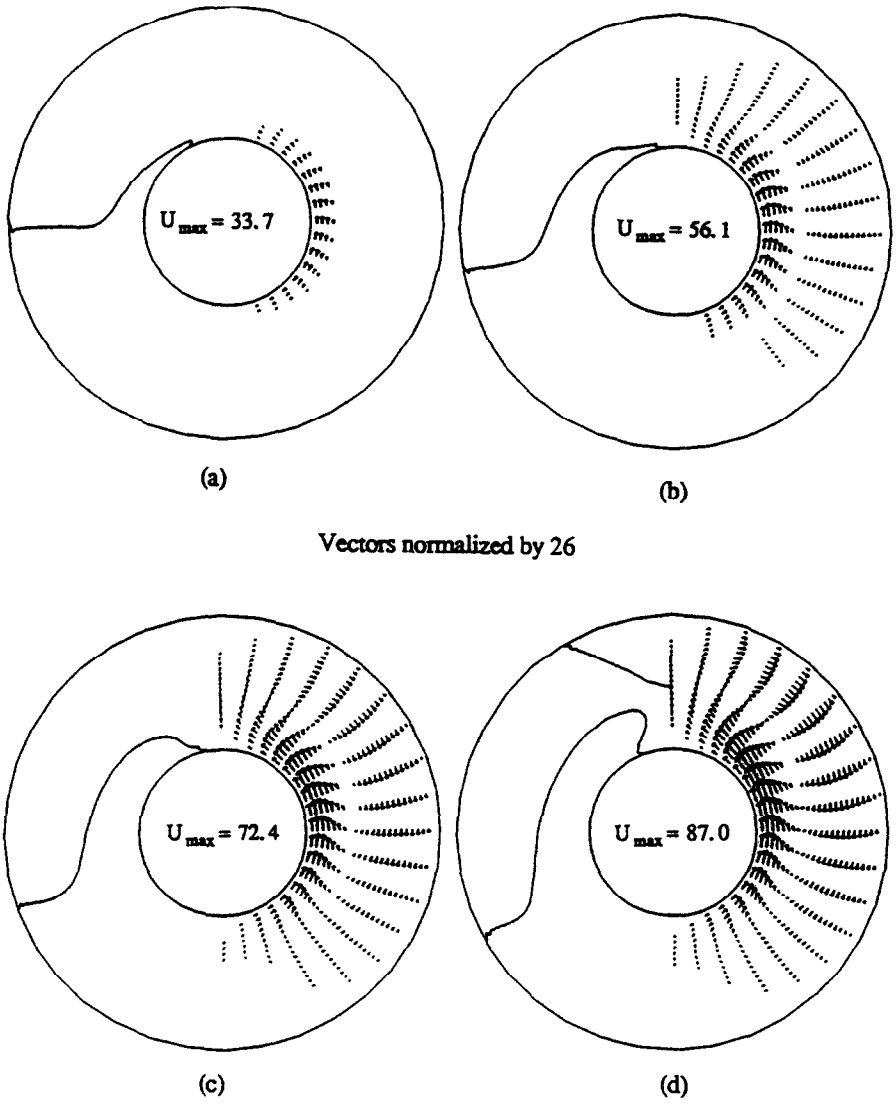

FIG. 8. Flow patterns for $Ra = 4.3 \times 10^4$ and different time steps at $z = 3L/8$: (a) $t = 10\Delta t$; (b) $t = 20\Delta t$; (c) $t = 30\Delta t$; (d) $t = 40\Delta t$.

cylinder. As the fluid adjacent to the inner cylinder moves up, the thickness of the thermal boundary layer around the inner cylinder increases and it eventually separates from the upper part of the inner cylinder and is entrained within the hot buoyant plume on top of the inner cylinder. The energy transferred from the lower portion of the inner cylinder is carried by this buoyant plume to the top of the outer cylinder. This hot plume is subsequently entrained by the thermal boundary layer along the outer cylinder as it is carried downward in the negative angular direction. The fluid within the thermal boundary layer along the outer cylinder loses energy as it moves down and consequently the thermal boundary layer separates from the outer cylinder at about $\phi \approx \pi/3$. The separation of the inner and outer cylinder thermal boundary layers results in the radial temperature inversion which is seen in Fig. 2. This phenomenon, of course, is due to the strong recirculating nature of the flow field. Based on these figures it can be deduced that the core region essentially spans a region which is approximately given by $L/4 < z < 3L/4$. Comparing Fig. 2 with the corresponding figure for $Ra = 4.3 \times 10^3$ (not presented here for brevity), it is found that, as expected, the extent of the core region within which the temperature distribution is independent of the axial position decreases with an increase in the Rayleigh number.

The flow field for $Ra = 4.3 \times 10^4$ at a plane adjacent to the left end wall and the mid axial plane are presented in Figs. 3(a) and (b), respectively. The maximum values of the velocity vectors in the R–ϕ plane at the above locations are 59.9 and 78.5, respectively. The velocity vectors are normalized by a

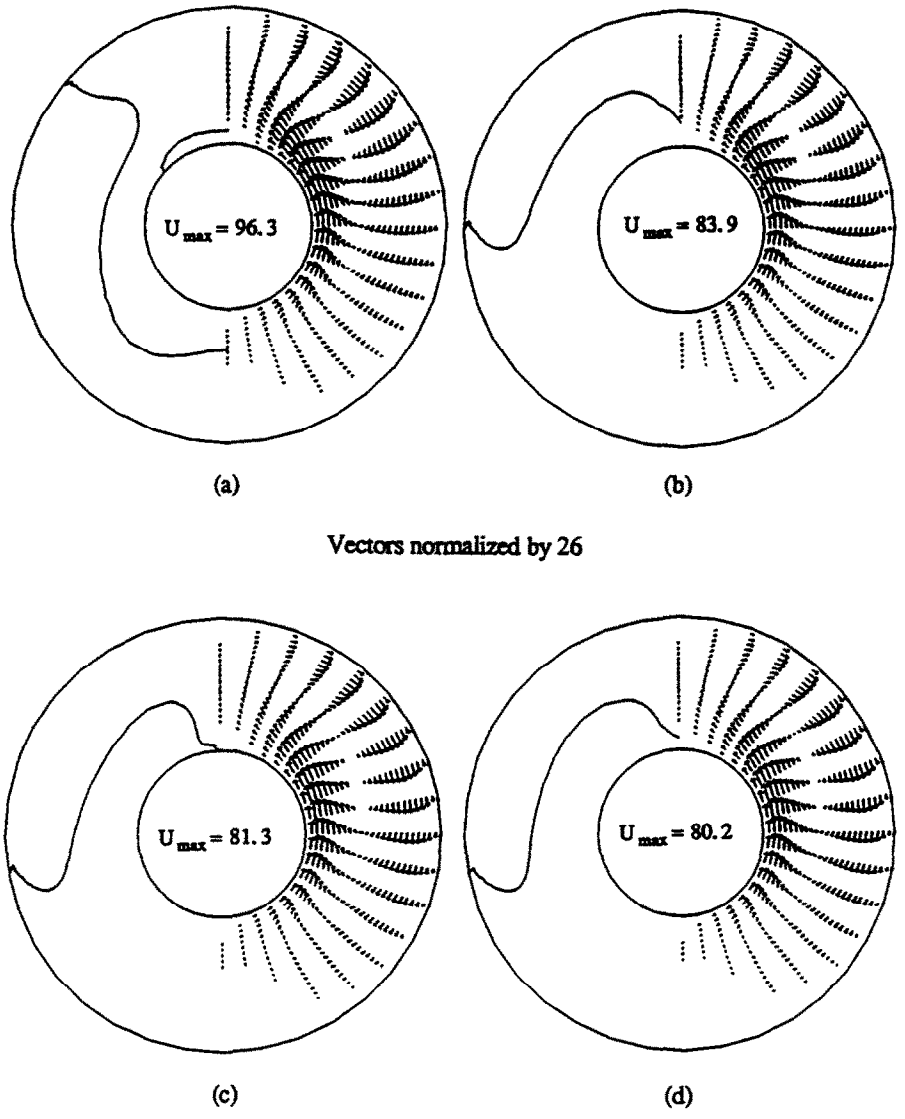

FIG. 9. Flow patterns for $Ra = 4.3 \times 10^4$ and different time steps at $z = 3L/8$: (a) $t = 50\Delta t$; (b) $t = 100\Delta t$; (c) $t = 150\Delta t$; (d) $t = 200\Delta t$.

factor of 26 to avoid clustering them together. Again, in here as in all other related figures, velocity vectors with a magnitude of less than 0.01 are not plotted. The maximum values of axial velocities in Figs. 3(a) and (b) are 14 and 0.01 while, their minimum values are -24 and -0.01, respectively. The contour values for the axial velocity are incremented by 4 in this case. As shown in these figures, the R–ϕ flow field is considerably retarded near the wall whereas the axial velocities nearly vanish around the mid axial plane.

The distributions of local Nusselt number for $Ra = 4.3 \times 10^4$ are presented in Figs. 4(a) and (b), respectively. As can be seen, aside from the regions close to the axial boundaries, the inner cylinder Nusselt number is almost independent of the axial coordinate, z. Close to the axial boundaries, the core value of the inner cylinder Nusselt number is reduced by about 5.5% at the lower angular symmetry plane, $\phi = 0$, while, it is reduced by about 22% at the upper angular symmetry plane, $\phi = \pi$. The core region for the outer cylinder Nusselt number is significantly reduced covering only 1/3 of the axial length. However, it should be noted that, the outer cylinder Nusselt number at the lower angular symmetry plane, $\phi = 0$, is almost independent of the axial direction. Its core value reduces only by 0.7% at the end walls. Figure 4(b) also shows that the outer Nusselt number goes through several maxima around the upper angular symmetry plane, $\phi = \pi$. This phenomenon is due to the presence of a strong three-dimensional flow field outside the core region.

To substantiate the above-mentioned phenomenon the velocity fields at four axial locations are presented in Figs. 5(a)–(d). These axial locations are at $z = 3\Delta z$,

$6\Delta z$, $8\Delta z$, and $17\Delta z$. The maximum values of axial velocities are 18, 11, 7.6, and 4.5, while their minimum values are -24, -11, -11, and -4.9, respectively. The axial velocity contours are incremented by 4 and displayed on the left-hand side of these figures. Comparison of the flow fields in the upper parts of Figs. 5(a) and (b) shows that the magnitude of the radial velocity which is responsible for the formation of the hot buoyant plume has decreased in the axial direction. Similarly, the contours of the axial velocity also indicate a substantial decrease in the axial direction. Consequently, the heat transfer from the upper part of the outer cylinder reduces considerably. On the other hand, a close examination of Figs. 5(b) and (c) reveals that the magnitude of the radial and axial velocities in the upper part of the buoyant plume has this time experienced an increase. Therefore, over this portion of the z-axis the heat transfer from the upper part of the outer cylinder increases. Finally, comparison of Figs. 5(c) and (d) indicates that the radial velocity in the plume remains almost unchanged whilst the axial velocity is reduced along the axial direction. Therefore, over this portion of the z-axis the heat transfer from the upper part of the outer cylinder is slightly decreased. It is this complex variation in the three-dimensional flow field which is directly responsible for the variations of the Nusselt number shown in Fig. 4(b).

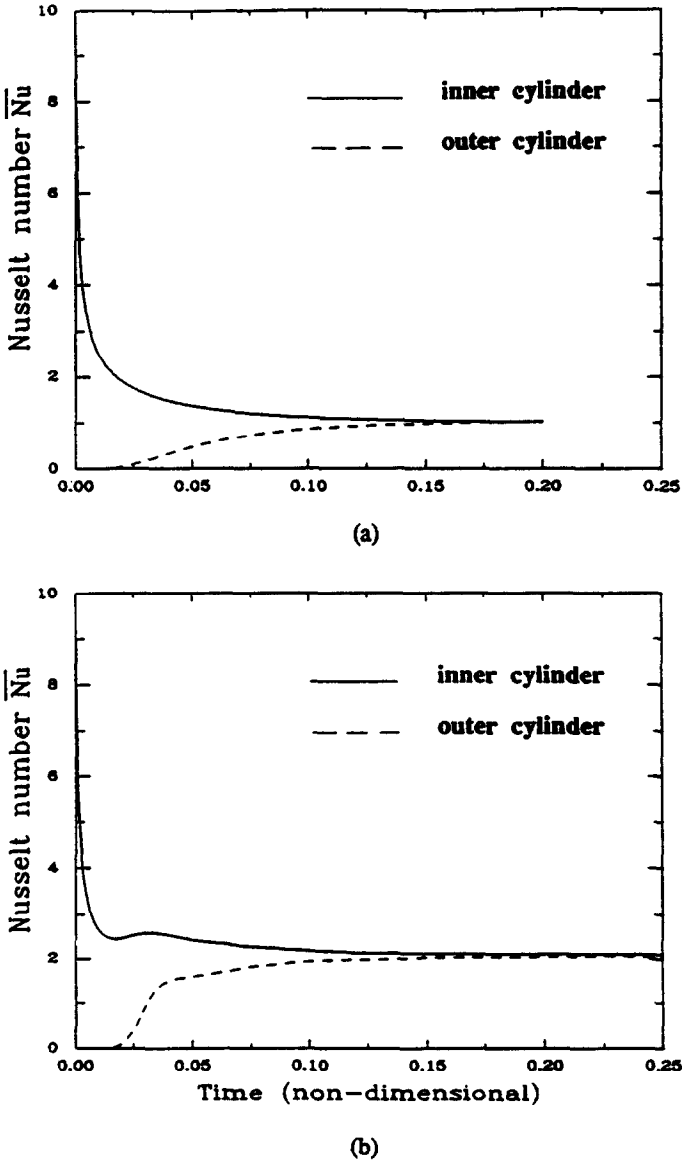

FIG. 10. Temporal variations of the mean Nusselt number at mid axial plane for different Rayleigh numbers: (a) $Ra = 4.3 \times 10^3$; (b) $Ra = 4.3 \times 10^4$.

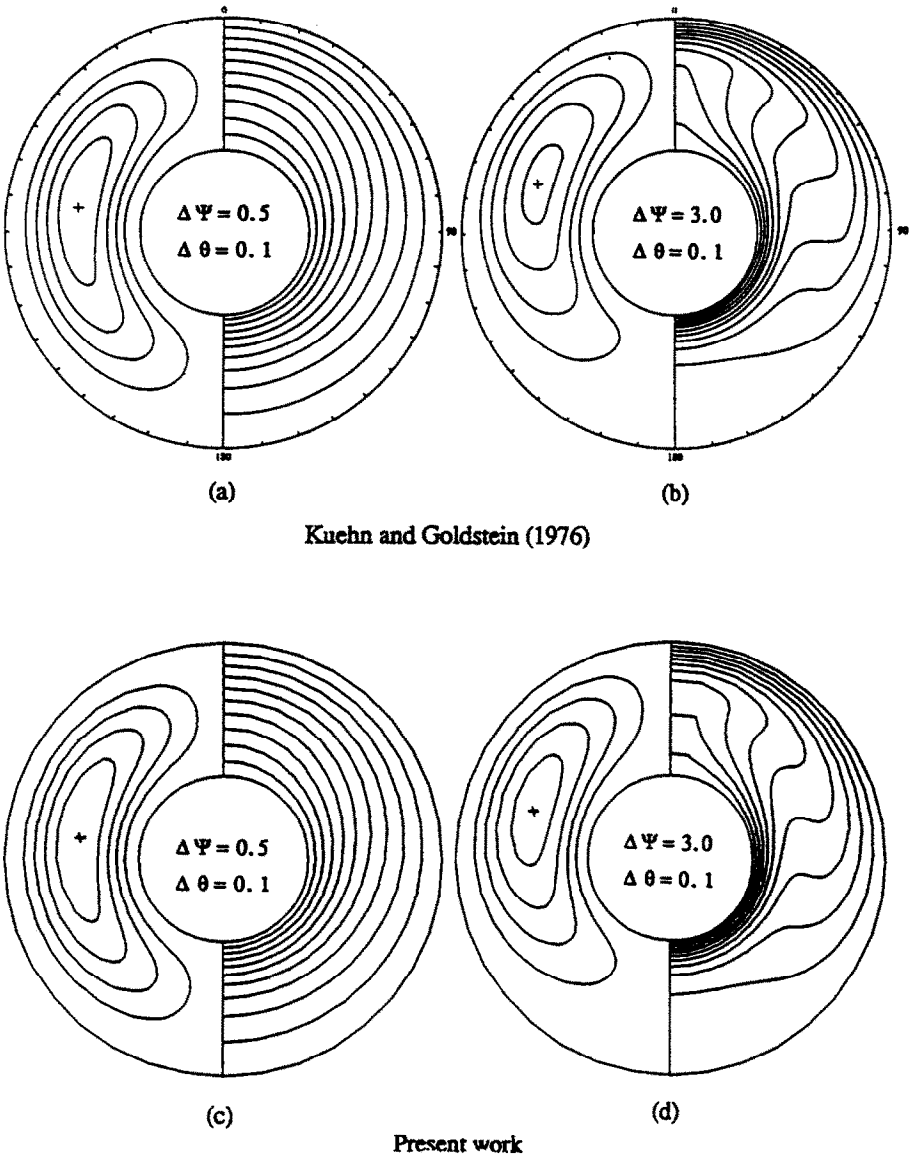

FIG. 11. Comparison of the streamlines and isotherms for different Rayleigh numbers: (a) and (c) $Ra = 4.3 \times 10^3$; (b) and (d) $Ra = 4.3 \times 10^4$.

3.1. *Transient results*

Figures 6–9 show the transient response of the flow and temperature fields for $Ra = 4.3 \times 10^4$ at an axial position which is 3/8 of the annulus length away from the left end wall. The temperature distributions on this plane at different times are displayed on the right-hand side of Figs. 6 and 7 while the corresponding isotherms at the mid axial plane are shown on the left portion of these figures. Here, the isotherms are incremented by 0.1 from their minimum value of 0.0 at the outer cylinder surface to their maximum value of 1.0 at the inner cylinder surface. The flow patterns at this plane for the same time steps are presented in Figs. 8 and 9. The maximum values of axial velocity are 1.6×10^{-4}, 3.1×10^{-4}, 5.5×10^{-4}, 9.7×10^{-4}, 2.1×10^{-3}, 4.1×10^{-2}, 2×10^{-1}, and 6.4×10^{-1} while their minimum values are -1.6×10^{-4}, -2.9×10^{-4}, -5.5×10^{-4}, -1×10^{-3}, -1.4×10^{-3}, -3.6×10^{-2}, -2.1×10^{-1}, and -6.9×10^{-1}, respectively. Since this axial position is located inside the core region within which the flow is essentially two-dimensional, its associated axial velocities are almost negligible when compared to the magnitude of the velocity vectors in the R–ϕ plane. It should be noted that, the solid line on the left portion of the above figures divides the regions within which the direction of axial velocity is either into or out of the R–ϕ plane.

In the early stages of flow development ($0 \leqslant t \leqslant 20\Delta t$), conduction is the dominant heat transfer mechanism inside the annulus as indicated by the shapes of the isotherms in Figs. 6(a) and (b). As seen in Figs. 8(a) and (b) during this period, the recirculating flow

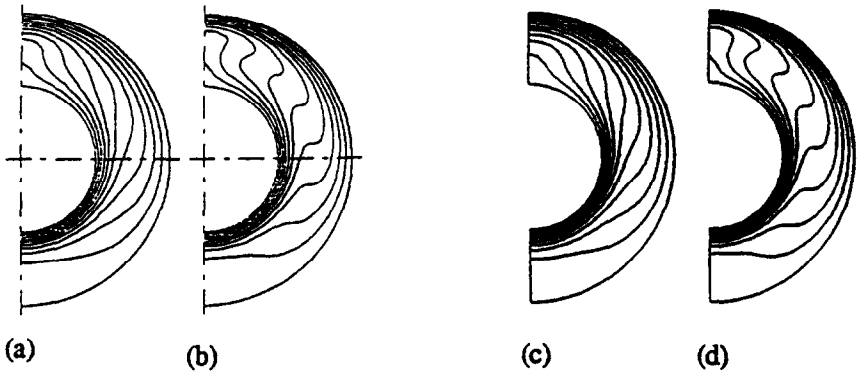

FIG. 12. Comparison of isotherms for $Ra = 10^5$, $Pr = 5 \times 10^3$ at different axial planes: (a) and (c) end wall; (b) and (d) mid axial plane.

has not picked up enough momentum to initiate a substantial transfer of energy from the inner cylinder to other regions of the annulus. For later times ($30\Delta t \leqslant t \leqslant 40\Delta t$), the recirculating flow in the R–ϕ plane becomes strong enough to increase the temperature of the fluid inside the annulus (Figs. 6(c), (d), 8(c) and (d)). The strength of the recirculating flow reaches its peak around $t = 50\Delta t$, whereas, seen by the flow structure in Fig. 9(a), the maximum value of the velocity vectors in the R–ϕ plane is achieved. After this time, due to an increase in the overall temperature of fluid in the upper part of the annulus, the strength of the recirculating flow begins to gradually decrease in time as seen by a close examination of the flow patterns in Figs. 9(b)–(d). This gradual decline continues up to a point in time after which, no further changes in the strength of the recirculating flow is observed. It is this recirculating flow which produces the temperature inversion which is observed in Figs. 7(b)–(d). It should be noted that, for this case, the steady state solution was reached at about $t = 500\Delta t$.

4. ACCURACY OF THE NUMERICAL SCHEME AND COMPARISON WITH PREVIOUS RESULTS

Aside from the detailed investigations, which were described earlier, on grid and time step independence several other tests and comparisons were performed. First, a case in which both cylinders were kept at constant and equal temperature was investigated. Obviously, the analytical steady state solution for this case is an isothermal fluid having the same temperature as that of the cylinders throughout the annulus. The numerical scheme provided an almost identical result.

To further check the accuracy as well as the convergence of the numerical scheme, the mean Nusselt numbers at the inner and outer cylinders were compared. The mean Nusselt number is defined as the angular average of its local values at the mid axial plane (equations (28) and (29)). The temporal variations of the mean Nusselt numbers for $Ra = 4.3 \times 10^3$ and 4.3×10^4 are presented in Figs. 10(a) and (b), respectively. The solid line represents the inner cylinder mean Nusselt number while the dotted line is used for the outer cylinder. As seen in Fig. 10 the inner cylinder mean Nusselt number experiences a decrease in time and the outer cylinder mean Nusselt number experiences an increase followed by their approach to a common steady state value. It should be noted that, in theory for a purely two-dimensional flow field, based on a simple energy balance, their asymptotic values should converge to the same value. As shown in Fig. 10(a) for $Ra = 4.3 \times 10^3$, the deviation is so small that it cannot be visually detected. For $Ra = 4.3 \times 10^4$, the relative difference between the inner and outer mean Nusselt numbers at steady state was found to be less than 1%.

The first set of comparisons was done with the results reported by Kuehn and Goldstein [1]. Figures 11(a) and (b) which are reproduced from their work, represent the streamlines and isotherms for $Ra = 4.3 \times 10^3$ and 4.3×10^4, respectively. Our corresponding three-dimensional solutions at the mid axial plane and at steady state are presented in Figs. 11(c) and (d). Comparison of the above figures shows an excellent agreement between the flow field and the temperature distribution. It should be noted that even locations of centers of rotation are in agreement. The inner and outer cylinder mean Nusselt numbers in the cited reference were also compared with the mid axial plane Nusselt numbers in the present study. Again, the comparison showed an excellent agreement with less than 0.5% deviation in the results.

The second set of bench marking was done with the results reported by Takata *et al.* [5]. They had investigated the steady state three-dimensional natural convection in a horizontal annulus for only one very large Prandtl number. Specifically, their three-

dimensional solution was based on a Prandtl number of 5000 in an annulus with radius ratio of $R_2/R_1 = 2$, length to radius ratio of $L/R_2 = 2$, and Rayleigh number of $Ra = 10^5$. Figures 12(a) and (b) show the isotherms at the end wall and the mid axial plane, reproduced from their work. The isotherms at the corresponding locations generated in the present work are shown in Figs. 12(c) and (d). As it can be seen, the computed results through our transient simulation are in excellent agreement with the steady state results reported by Takata *et al.* [5].

5. CONCLUSIONS

Transient three-dimensional buoyancy induced flow and heat transfer in a closed horizontal annulus was numerically investigated. A detailed analysis of the three-dimensional flow and temperature fields was presented and the effects of the impermeable end walls on the flow field were discussed. The existence and validity of a two-dimensional solution was explored and the presence of a core region was established. Various aspects of the three-dimensional dependency of the Nusselt number were presented and discussed. Finally, the formation of the complex flow and temperature fields as a result of the sudden heating of the inner cylinder was analyzed.

Acknowledgement—The grant from Ohio Supercomputer Center is acknowledged and appreciated.

REFERENCES

1. T. H. Kuehn and R. J. Goldstein, An experimental and theoretical study of natural convection in the annulus between horizontal concentric cylinders, *J. Fluid Mech.* **74,** 695–719 (1976).
2. A. Aziz and J. D. Hellums, Numerical solution of the three-dimensional equations of motion for laminar natural convection, *Physics Fluids* **10,** 314–324 (1967).
3. H. Ozoe, T. Okamoto and S. W. Churchill, Natural convection in a vertical annular space heated from below, *Heat Transfer—Jap. Res.* **8,** 82–93 (1979).
4. H. Ozoe, T. Shibata and S. W. Churchill, Natural convection in an inclined circular cylindrical annulus heated and cooled on its end plates, *Int. J. Heat Mass Transfer* **24,** 727–737 (1981).
5. Y. Takata, K. Iwashige, K. Fukuda and S. Hasegawa, Three-dimensional natural convection in an inclined cylindrical annulus, *Int. J. Heat Mass Transfer* **27,** 747–754 (1984).
6. T. Fusegi and B. Farouk, A three-dimensional study of natural convection in the annulus between, horizontal concentric cylinders, *Proc. 8th Int. Heat Transfer Conf.*, Vol. 4, pp. 1575–1580 (1986).
7. J. Douglas, On the numerical integration of $U_{xx} + U_{yy} = U_t$ by implicit methods, *J. Soc. Ind. Appl. Math.* **3,** 42–65 (1955).
8. J. Douglas, Alternating direction methods for three space variables, *Numer. Math.* **4,** 41–63 (1962).
9. J. Douglas and H. H. Rachford, On the numerical solution of heat conduction problems in two and three space variables, *Trans. Am. Math. Soc.* **82,** 421–439 (1956).
10. G. J. Hirasaki and J. D. Hellums, A general formulation of the boundary conditions on the vector potential in three-dimensional hydrodynamics, *Q. Appl. Math.* **26,** 331–342 (1968).
11. J. Ettefagh and K. Vafai, Natural convection in open-ended cavities with a porous obstructing medium, *Int. J. Heat Mass Transfer* **31,** 673–693 (1988).
12. P. L. T. Brian, A finite-difference method of high-order accuracy for the solution of three-dimensional transient conduction problems, *A.I.Ch.E. Jl* **7,** 367–370 (1961).
13. Y. T. Tsui and B. Tremblay, Transient natural convection heat transfer in the annulus between concentric, horizontal cylinders with isothermal surfaces, *Int. J. Heat Mass Transfer* **27,** 103–111 (1984).

ETUDE DE L'ECOULEMENT NATUREL TRIDIMENSIONNEL, VARIABLE ET DU TRANSFERT THERMIQUE DANS UN ESPACE ANNULAIRE FERME ET HORIZONTAL

Résumé—On étudie numériquement l'écoulement de convection naturelle et le transfert thermique dans un espace annulaire horizontal limité par deux frontières imperméables dans la direction axiale. On présente une analyse tridimensionnelle variable des effets de bout sur le transfert thermique et l'écoulement correspondant. Les effets des frontières imperméables sont caractérisés par un retardement du champ d'écoulement à cause du frottement visqueux dans les régions proches des bouts. Les résultats pour l'air et un rapport des rayons égal à 2,6 montrent que la distribution de température reste inchangée dans le coeur pourvu que le rapport de la longueur de l'anneau au rayon externe soit supérieur à 4. Les champs de vitesse et de température sont symétriques par rapport au plan vertical médian de l'anneau. On présente quelques configurations intéressantes résultant du brusque chauffage du cylindre intérieur. On considère enfin la formation des champs de vitesse et de température à la suite du brusque chauffage du cylindre intérieur.

UNTERSUCHUNG DER INSTATIONÄREN DREIDIMENSIONALEN AUFTRIEBSSTRÖMUNG UND DES WÄRMEÜBERGANGS IN EINEM GESCHLOSSENEN HORIZONTALEN RINGRAUM

Zusammenfassung—In dieser Arbeit werden die Strömung und der Wärmeübergang bei natürlicher Konvektion in einem waagerechten Ringraum untersucht, der in axialer Richtung durch zwei undurchlässige Begrenzungen abgeschlossen ist. Der Einfluß der Endeffekte auf den Wärmeübergang und das entsprechende Strömungsfeld wird analytisch untersucht (instationär, dreidimensional). Der Einfluß der undurchlässigen Endflächen ist durch eine Verzögerung des Strömungsfeldes gekennzeichnet, die durch die viskosen Scherkräfte in den Endregionen hervorgerufen wird. Die Ergebnisse für Luft und ein Radienverhältnis von 2,6 zeigen, daß die Temperaturverteilung im Kernbereich unverändert bleibt, vorausgesetzt, daß das Verhältnis von Länge zu äußerem Radius des Ringraums größer als 4 ist. Die Strömungs- und Temperaturfelder sind bezüglich der axialen Mittelebene des Ringraums symmetrisch. Bei einer plötzlichen Beheizung des inneren Zylinders ergibt sich eine Reihe interessanter Gesichtspunkte. Abschließend erfolgt eine ausführliche Darstellung der Entwicklung von Strömungs- und Temperaturfeldern in der Folge der plötzlichen Beheizung des inneren Zylinders.

ИССЛЕДОВАНИЯ НЕСТАЦИОНАРНОГО ТРЕХМЕРНОГО ТЕЧЕНИЯ, ВЫЗВАННОГО ПОДЪЕМНОЙ СИЛОЙ, И ТЕПЛОПЕРЕНОСА В ЗАМКНУТОМ ГОРИЗОНТАЛЬНОМ КОЛЬЦЕВОМ КАНАЛЕ

Аннотация—Численно исследуются вызванное подъемной силой течение и теплоперенос в горизонтальном кольцевом канале с двумя непроницаемыми границами в осевом направлении. Представлены нестационарный трехмерный анализ влияния торцов на теплоперенос и соответствующее поле течения. Показано, что эффекты аксиальных непроницаемых границ выражаются в замедлении поля течения за счет сдвиговой силы вязкого сопротивления на участке у торцевых стенок. Результаты, полученные для воздуха в случае отношения радиусов, равного 2,6, показывают, что распределение температур в области ядра остается постоянным при условии, что отношение длины канала к внешнему радиусу больше 4. Найдено, что поля течения и температур являются симметричными относительно осевой плоскости канала. Приводятся некоторые интересные особенности, связанные с внезапным нагревом внутреннего цилиндра. Детально анализируется также формирование полей течения и температур в результате этого нагрева.